Nuclear Engineering and Technology 52 (2020) 2410–2414

Contents lists available at ScienceDirect

Nuclear Engineering and Technology

journal homepage: www.elsevier.com/locate/net

Technical Note

Evaluation of dose distribution from ^{12}C ion in radiation therapy by FLUKA code

Jamshid Soltani-Nabipour [a], Abdollah Khorshidi [a, b, *], Faezeh Shojai [c], Khazar Khorami [d]

[a] Department of Medical Radiation Engineering, Islamic Azad University, Parand Branch, P.O. Box: 3761396361, Tehran, Iran
[b] School of Paramedical, Gerash University of Medical Sciences, P.O. Box: 7441758666, Gerash, Iran
[c] Faculty of Engineering, Islamic Azad University, Science and Research Branch, P.O. Box: 1477893855, Tehran, Iran
[d] Department of Physics, Islamic Azad University, Central Tehran Branch, P.O. Box: 1469669191, Tehran, Iran

ARTICLE INFO

Article history:
Received 28 December 2019
Received in revised form
18 February 2020
Accepted 11 March 2020
Available online 14 March 2020

Keywords:
Carbon ions
Soft tissue
Water
Bone
Bragg peak
FLUKA

ABSTRACT

Heavy ions have a high potential for destroying deep tumors that carry the highest dose at the peak of Bragg. The peak caused by a single-energy carbon beam is too narrow, which requires special measures for improvement. Here, carbon-12 (^{12}C) ion with different energies has been used as a source for calculating the dose distribution in the water phantom, soft tissue and bone by the code of Monte Carlo-based FLUKA code. By increasing the energy of the initial beam, the amount of absorbed dose at Bragg peak in all three targets decreased, but the trend for this reduction was less severe in bone. While the maximum absorbed dose per bone-mass unit in energy of 200 MeV/u was about 30% less than the maximum absorbed dose per unit mass of water or soft tissue, it was merely 2.4% less than soft tissue in 400 MeV/u. The simulation result showed a good agreement with experimental data at *GSI* Darmstadt facility of biophysics group by 0.15 cm average accuracy in Bragg peak positioning. From 200 to 400 MeV/u incident energy, the Bragg peak location increased about 18 cm in soft tissue. Correspondingly, the bone and soft tissue revealed a reduction dose ratio by 2.9 and 1.9. Induced neutrons did not contribute more than 1.8% to the total energy deposited in the water phantom. Also during ^{12}C ion bombardment, secondary fragments showed 76% and 24% of primary 200 and 400 MeV/u, respectively, were present at the Bragg-peak position. The combined treatment of carbon ions with neutron or electron beams may be more effective in local dose delivery and also treating malignant tumors.

1. Introduction

Each charged particle has a specific range inside the matter. They interact with each other in the course of incident particles paths and cause ionization. When their velocity decreases, their ability to interact and ionize increases. So, a peak corresponding to the particle energy in the depth of the target material is created. This peak with the highest delivered dose is called Bragg peak. Heavy ions have a very high potential for eliminating deep tumors. However, due to their limited energy in the tail produced by induced low-Z fragments [1], they are not harmful to the healthy tissue adjacent to the cancerous cells, unlike the other radiation used in traditional therapies by electron [2], proton [3–7], X-ray [8] and neutron beams [9–12]. The FLUKA Monte Carlo-based code is a precision instrument in simulating the transport of heavy particles within matter. In this study using this code, the Bragg peak is investigated for delivered dose of incident ^{12}C in water, soft tissue and bone.

2. Materials and methods

FLUKA is a general-purpose computer code that has been written especially for calculating the quantities associated with particles passing through the material and their interactions, based on the Monte Carlo method. In this case according to Fig. 1, the target material was simulated as a cylindrical phantom of water with a radius of R = 5 cm and a height of H = 40 cm, which is located inside a larger cylinder covered with air. These dimensions have been selected according to the approximate dimensions of a typical tumor, as well as the range of ^{12}C ions in water. The carbon beam from a single energy source outside the cylinder is radiated in the direction of the main axis and entered the cylinder.

* Corresponding author. Department of Medical Radiation Engineering, Islamic Azad University, Parand Branch, P.O. Box: 3761396361, Tehran, Iran.
E-mail addresses: abkhorshidi@contact.publons.com, abkhorshidi@chmail.ir (A. Khorshidi).

https://doi.org/10.1016/j.net.2020.03.010

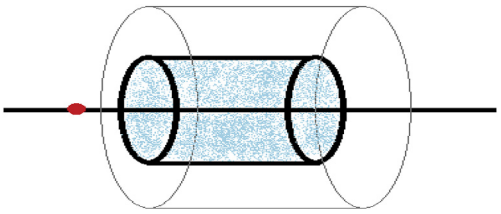

Fig. 1. The water target embedded in an airtight cylinder, and carbon beam is radiated from a Gaussian source (red point) along the cylinder axis. (For interpretation of the references to colour in this figure legend, the reader is referred to the Web version of this article.)

To match the simulated geometry with the experimental study performed at *GSI* Darmstadt facility of biophysics group [13], the Gaussian radiation source with 5 mm FWHM was considered. In the definition of the simulation parameters, the Hadron-Therapy default values of the code were used in the particle tracking process. To qualitatively investigate this problem, the three different energies of ^{12}C beams at 200, 300, and 400 MeV/u were simulated in several different target materials of water, soft tissue and bone. In the standard defined by ICRU used in these simulations, the soft tissue and water density is 1 g/cm^3 and the bone density is 1.85 g/cm^3. In this standard, the soft tissue consists of four elements: oxygen (0.762), carbon (0.111), hydrogen (0.10) and nitrogen (0.026).

3. Results

Figs. 2–4 compare the absorbed dose in water phantom, soft tissue and bone targets at three different energies of ^{12}C by 200, 300 and 400 MeV/u. The falling of the dose attribute was the same within the water and soft tissue for all energies used, and the location of Bragg point was almost identical for these two materials. Also, the amounts of absorbed dose in the intake region were approximately the same for all three targets and for all energy sources.

By increasing the energy of the initial beam, the amount of absorbed dose in the Bragg peak decreased in all three targets, but the trend for this reduction was less severe in the bone. So, while the maximum absorbed dose per unit bone mass at 200 MeV/u was about 30% less than the maximum absorbed dose per unit mass of water or soft tissue, it was only 2.4% less than soft tissue at 400 MeV/u. The maximum absorbed dose per primary in bone was nearly 0.0082, 0.0065 and 0.0045 GeV/g for 200, 300 and 400 MeV/u, respectively. Correspondingly, these amounts in soft tissue were 0.0130, 0.0074 and 0.0045 GeV/g. The bone and soft tissue revealed a reduction dose ratio by 2.9 and 1.9 from 200 to 400 MeV/u incident energy, respectively.

Also, Table 1 shows the Bragg peak location inside the water, bone and soft tissue for different radiating energies of ^{12}C. The accuracy of the simulation was between 0.10 and 0.20 cm.

In general, as the energy of the primary ion increases, the peak position is transferred to the deeper parts of the target material. For carbon beams with the energy of 200 MeV/u, the position of Bragg peak was 8.68 cm inside the soft tissue and 4.93 cm inside the bone. By increasing the energy of the primary beams to 400 MeV/u, the distance between peak position and the entrance of the beam into soft tissue (27.53 cm) and bone (15.8 cm) increased almost by 18 and 11 cm, respectively.

Radiation therapy using other heavy ions like proton creates secondary and induced particles through nuclear interactions across dissimilar tissues. The derived particle spectrum depends on the tissue composition, charges as well as the energy of the incoming beam. In proton radiation therapy, analytical radiobiological models typically use linear energy transfer (LET) and absorbed dose. Here, in comparison with incident 200 MeV protons in 40 cm^3 water phantom, the induced neutrons were evaluated as shown in Fig. 5. The obtained spectrum was normalized to incident beam and involved all induced neutrons in 4π space. By incoming ^{12}C beam on the water phantom, the proportions of deposited energy into the phantom with and without considering induced neutrons were 84% and 82%, respectively. The difference between considering induced neutrons was 2% higher than excluding ones.

In addition to that, the obtained absorbed doses from induced neutrons (D) multiplied by mean relative biological effectiveness (RBE) were 0.38% and 0.93% for ^{12}C and proton beams, correspondingly.

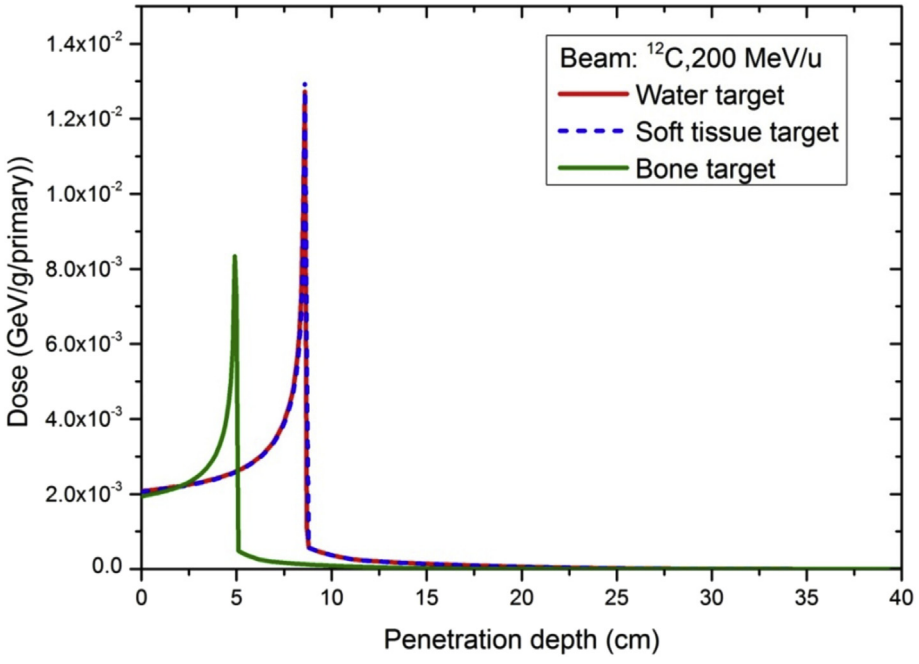

Fig. 2. The total absorbed dose versus depth inside water, tissue and bone at 200 MeV/u of incident ^{12}C beam.

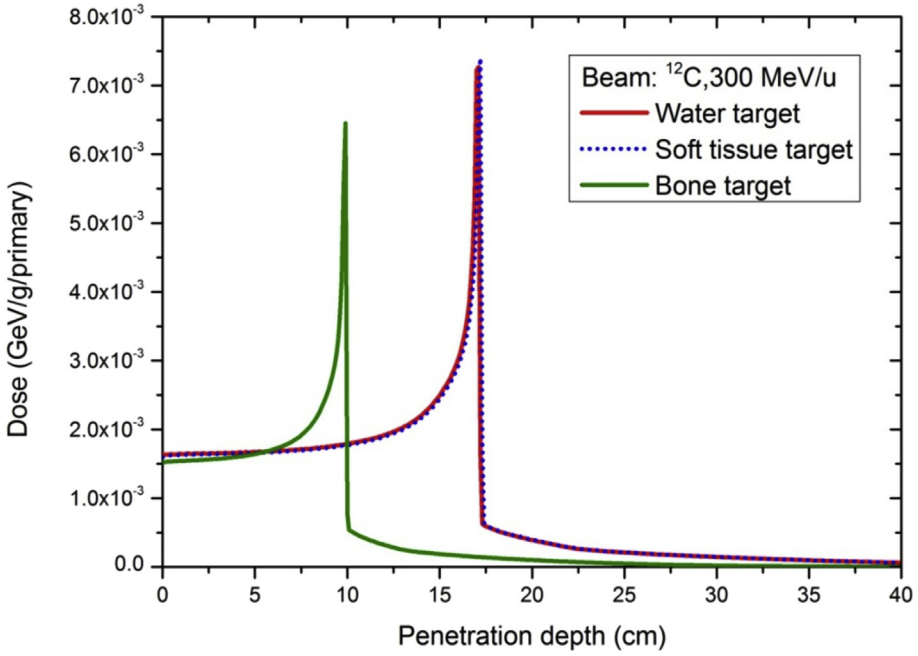

Fig. 3. The total absorbed dose versus depth inside water, tissue and bone at 300 MeV/u of incident ^{12}C beam.

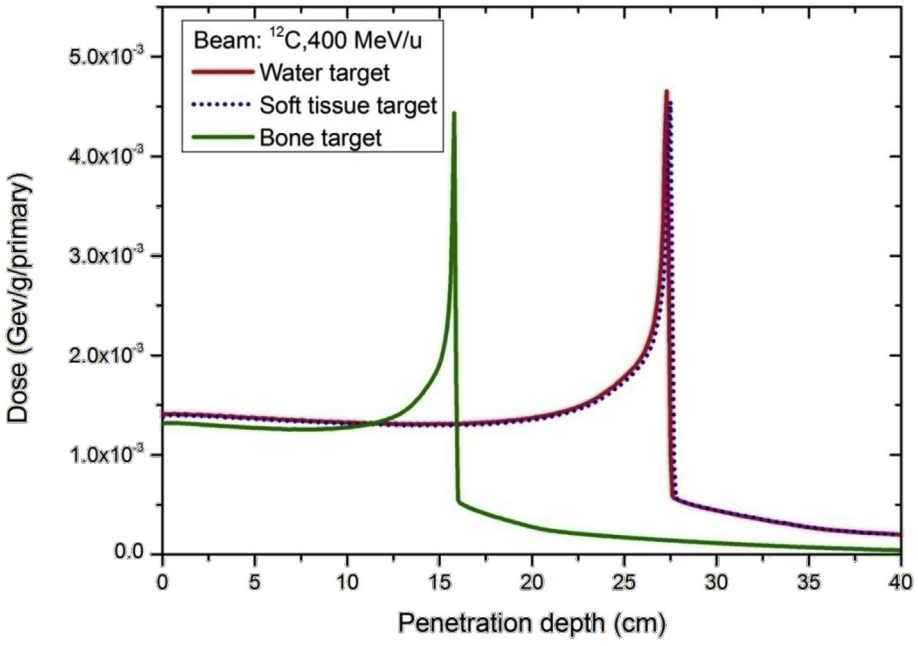

Fig. 4. The total absorbed dose versus depth inside water, tissue and bone at 400 MeV/u of incident ^{12}C beam.

Table 1
Location of Bragg peak in three targets from carbon beam at different energies.

Incident energy (MeV/u)	Depth (cm) in different materials		
	water phantom	soft tissue	bone
200	8.64	8.68	4.93
300	17.11	17.22	9.87
400	27.34	27.53	15.85

The secondary particles and other fragments generated have a small fraction in the Bragg-peak shift. Therefore, another simulation was carried out to estimate the generated secondary fragments—hydrogen, alpha particles, lithium and boron—under ^{12}C ion bombardment. The outcomes showed that 76% of the initial 200 MeV/u^{12}C ions are present at the Bragg-peak location, while this proportion inclined to 24% for 400 MeV/u.

4. Discussion

In addition to the different atomic numbers and densities of the compositions of bone and soft tissue, the difference in ionization potential (I = 74.9 eV for soft tissue and I = 91.9 eV for bone) is also

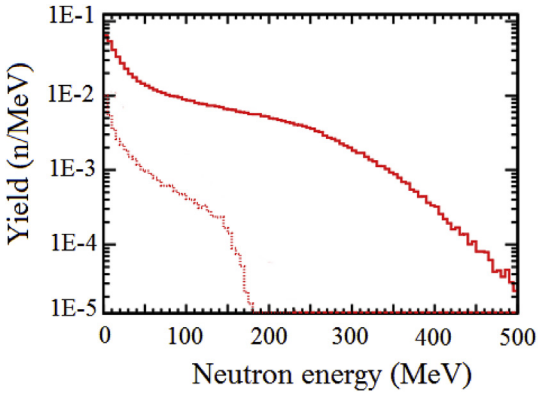

Fig. 5. Induced neutron spectrum derived from 300 MeV/u of incident ^{12}C ion beam (solid line) in comparison with 200 MeV incident proton beam (dash line) inside 40 cm^3 water phantom.

a reason for different beam behavior in these two substances [14]. The elements with low ionization potential, the amount of energy required to separate an electron from an atom, easily lose electrons and become cationic. The carbon-ion radiotherapy has superior dose compliance in the treatment of deep-seated malignant tumors compared to conventional X-ray radiotherapy. Also, ^{12}C ion beam has a higher relative biological effectiveness compared to proton or X-ray beams [15–17]. Meanwhile, ^{12}C beams have several biological benefits regarding high linear energy transfer including reduced oxygenation ratio, weakened ability to repair sub-lethal and potentially lethal damage, and lessened cell cycle dependent radiation sensitivity compared to those discerned with X-rays or proton beams. However shielding of the heavy-ion medical accelerator is a basic requirement [18,19], the X-ray fluoroscopy or radiography device and electron generators can accompany the treatment planning by iso-center method in positioning to reduce or exclude the extra clinical examination [2,20–24]. Furthermore, multi-modality therapy such as conventional radiotherapy, boron neutron capture therapy (BNCT) and concomitant chemotherapy can be normalized for various advanced cancers [11,16,25]. Conversely, increased toxicity and recurrence are still two main problems to conquer. In addition to that, ^{12}C therapy provides the opportunity to show potential competences in combination with immunotherapy, surgical intervention, cytotoxic drugs and molecular agents to improve topical scrutinization, avert harsh poisonous and preserve the quality of life. On the other hand, the maximum dose transfer with the least damage to adjacent healthy tissues is one of the benefits of ^{12}C ion beam therapeutic approach. This property also has the proton therapy. However, the lateral drop around the tumor is steeper with ^{12}C beam than with proton beam [26]. At the end area of the curve tail, a small dose is deposited with carbon ions, while almost no dose is deposited with protons. This is because primary ^{12}C ions undergo distinct nuclear interactions and fragment into various particles by a lower atomic number, generating a fragmentation tail beyond the Bragg peak.

As the range of the particles —at same speed— scales with A/Z^2, the depth-dose profile of heavy-ion irradiations elucidates a distinctive fragment tail beyond the Bragg peak. For carbon ions the tail-dose is comparatively small, but considering the production of the induced isotopes and particles alters the dose distribution and also peak position. Since induced neutrons from radiation with heavy ions provide an additional absorbed dose, it was expected that their impacts on the Bragg peak would extend far beyond the acme. Therefore in this research, the stimulated neutronic dose was spread over a wider range, namely out of the normal range of depth-dose estimations. Kumamoto et al. [27], Gunzert-Marx et al. [28] and Khorshidi [9,29] have experimentally designed a neutron detector located behind the target under carbon or proton irradiations to measure the induced neutrons. Their outcomes demonstrated that the fragmentation of projectile nuclei and local energy deposition of charged hadrons are inevitable consequences for dose absorption. Here the parameter (average RBE $\times$ D) using incident ^{12}C ions showed a share of 0.38% in the deposited energy in the phantom. It was found that induced neutrons do not contribute more than 1.8% to the total energy deposited in the phantom. Also during ^{12}C ion bombardment, secondary fragments showed 76% and 24% of initial 200 and 400 MeV/u, respectively, were present at the Bragg-peak position.

As ^{12}C beam treatment planning and dose transfer systems continue to evolve, personalized cancer therapy is more meliorated in the next decade. In particular, the deformation and tumor shrinkage, management of organ movements as well as the image-controlled adaptive treatment strategy can improve the high precision of the energy deposition.

5. Conclusion

The energy deposition from ^{12}C beam raises with the depth of penetration towards the sharpest point at the end of its range, namely the Bragg peak. Since the acquired peak is too sharp and narrow to fully wrap the target lesion, the cancer treatment can be applied to the outspread peak by broadening methods in accordance with the dimension of the lesion. Compared to electron, neutron and photon therapy, the results from ^{12}C beam can be used to increase the localized radiation dose and energy delivery to tumors while reducing the exposure of adjacent normal tissues.

Summary of the article

Three targets (water phantom, soft tissue and bone) under the radiation of three different energies of ^{12}C ion beam (200, 300 and 400 MeV/u) were simulated by Monte Carlo-based FLUKA code. The Bragg peak position and dose distribution were compared. The bone and soft tissue demonstrated a reduction dose ratio by 2.9 and 1.9 with the increase in incident ion energy from 200 to 400 MeV/u, respectively. As the energy of the primary ion increased, the Bragg peak position was moved to the deeper parts of the target. Compared to electron, neutron, and photon therapy, the results of the ^{12}C beam can be used to increase the localized dose to tumor while reducing exposure of adjacent normal tissues.

Ethical approval

Not required.

Funding source

No Involvement.

Declaration of competing interest

The authors declare that they have no known competing financial interests or personal relationships that could have appeared to influence the work reported in this paper.

References

[1] J. Soltani-Nabipour, M.A. Popovici, G. Cata-Danil, Residual nuclides produced by 290 MeV/u 12C ions beam in a liquid water target, Rom. Rep. Phys. 62 (1) (2010) 37–46, doi: n/a.

[2] A. Khorshidi, A. Rajaee, M. Ahmadinejad, M. Ghoranneviss, M. Ettelaee, Low energy electron generator design and depth dose prediction for micro-superficies tumors treatment purposes, Phys. Scripta 89 (9) (2014), 095001, https://doi.org/10.1088/0031-8949/89/9/095001.
[3] P. Azimi, A. Movafeghi, Proton therapy in neurosurgery: a historical review and future perspective based on currently available new generation systems, Int. J. Clin. Neurosci. 3 (2) (2016) 59–80, https://doi.org/10.22037/icnj.v3i2.13324.
[4] S. Malmir, A. Asghar Mowlavi, S. Mohammadi, Enhancement evaluation of energy deposition and secondary particle production in gold nanoparticle aided tumor using proton therapy, Int. J. Canc. Manag. 10 (10) (2017), e10719, https://doi.org/10.5812/ijcm.10719.
[5] G.L. Campos, T.P.R. Campos, Proposed parameters for a circular particle accelerator for proton beam therapy obtained by genetic algorithm, Braz J. Radiol. Sci. 2 (7) (2019) 1–15, doi: n/a.
[6] E.A. Krasavin, A.V. Boreyko, M.G. Zadneprianetc, E.V. Ilyina, R.A. Kozhina, E.A. Kuzmina, E.A. Kulikova, E.V. Smirnova, G.N. Timoshenko, S.I. Tiounchik, V.N. Chausov, The influence of DNA synthesis inhibitors on the biological efficiency of the modified Bragg peak proton beam, PEPAN Lett. 16 (2) (2019) 181–190, doi: n/a.
[7] A. Khorshidi, Accelerator-based methods in radio-material 99Mo/99mTc production alternatives by Monte Carlo method: the scientific-expedient considerations in nuclear medicine, J. Multiscale Model. (JMM) 11 (1) (2020) 1930001, https://doi.org/10.1142/S1756973719300016.
[8] J.S. Nabipour, A. Khorshidi, Spectroscopy and optimizing semiconductor detector data under X and γ photons using image processing technique, J. Med. Imag. Radiat. Sci. 49 (2) (2018) 194–200, https://doi.org/10.1016/j.jmir.2018.01.004.
[9] A. Khorshidi, Neutron activator design for 99Mo production yield estimation via lead and water moderators in transmutation's analysis, Instrum. Exp. Tech. 61 (2) (2018) 198–204, https://doi.org/10.1134/S002044121802015X.
[10] A. Khorshidi, Gold nanoparticles production using reactor and cyclotron based methods in assessment of 196,198Au production yields by 197Au neutron absorption for therapeutic purposes, Mater. Sci. Eng. C 68 (2016) 449–454, https://doi.org/10.1016/j.msec.2016.06.018.
[11] A. Khorshidi, Radiochemical parameters of molybdenum-99 transmutation in cyclotron-based production method using a neutron activator design for nuclear-medicine aims, Eur. Phys. J. Plus 134 (2019) 249, https://doi.org/10.1140/epjp/i2019-12568-3.
[12] A. Khorshidi, A. Pazirandeh, Molybdenum transmutation via 98Mo samples using bismuth/lead neutron moderators, Europhys. Lett. 123 (1) (2018), 12001, https://doi.org/10.1209/0295-5075/123/12001.
[13] G. Battistoni, et al., The FLUKA code: description and benchmarking, in: AIP Conf. Proc., vol. 896, 2007, pp. 31–49. In Proceedings of the Hadronic Shower Simulation Workshop 2006, Fermilab 6–8 September 2006.
[14] P. Andreo, On the clinical spatial resolution achievable with protons and heavier charged particle radiotherapy beams, Phys. Med. Biol. 54 (2009) N205–N215, https://doi.org/10.1088/0031-9155/54/11/N01.
[15] T. Abe, T. Ohno, M. Koto, Y. Demizu, H. Suefuji, H. Tsuji, T. Okimoto, Y. Shioyama, J.I. Saitoh, K. Shirai, K. Nemoto, T. Nakano, T. Kamada, Japan Carbon-Ion Radiation Oncology Study Group. A multi-institutional retrospective study of carbon-ion radiotherapy for non-squamous cell malignant tumors of the nasopharynx: subanalysis of Japan Carbon-Ion Radiation Oncology Study Group study 1402 HN, Cancer Med. 7 (12) (2018) 6077–6083, https://doi.org/10.1002/cam4.1884.
[16] A. Khorshidi, Accelerator driven neutron source design via beryllium target and 208Pb moderator for boron neutron capture therapy in alternative treatment strategy by Monte Carlo method, J. Canc. Res. Therapeut. 13 (3) (2017) 456–465, https://doi.org/10.4103/0973-1482.179180.
[17] R. Reiazi, A. Norozi, M. Etedadialiabadi, A literature survey on cost-effectiveness of proton beam therapy in the management of breast cancer patients, Iran. J. Cancer Prev. 8 (6) (2015), e4373, https://doi.org/10.17795/ijcp-4373.
[18] M. Ashoor, A. Khorshidi, L. Sarkhosh, Appraisal of new density coefficient on integrated-nanoparticles concrete in nuclear protection, Kerntechnik 85 (1) (2020) 9–14, https://doi.org/10.3139/124.190016.
[19] J. Soltani-Nabipour, A. Khorshidi, F. Sadeghi, Constructing environmental radon gas detector and measuring concentration in residential buildings, Phys. Part. Nucl. Lett. 16 (6) (2019) 789–795, https://doi.org/10.1134/S154747711906030X.
[20] G. Khaleghi, J. Soltani-Nabipour, A. Khorshidi, F. Taheri, Design of band-pass filters by experimental and simulation methods at the range of 100-125 keV of X-ray in fluoroscopy, Int. J. Biosci. Technol. (2019), https://doi.org/10.1504/IJBET.2019.10025733. Inderscience Publishers - linking academia, business and industry through research In press.
[21] A. Khorshidi, B. Khosrowpour, S.H. Hosseini, Determination of defect depth in industrial radiography imaging using MCNP code and SuperMC software, Nucl. Eng. Technol. (2020), https://doi.org/10.1016/j.net.2019.12.010. In press.
[22] A. Khorshidi, Assessment of SPECT images using UHRFB and other low-energy collimators in brain study by Hoffman phantom and manufactured defects, Eur. Phys. J. Plus 135 (261) (2020), https://doi.org/10.1140/epjp/s13360-020-00238-6. In press.
[23] A. Khorshidi, A. Abdollahi, A. Pirouzi, S.H. Hosseini, Band pass filter plan in fluoroscopy for high energy range, SN Appl. Sci. 2 (2020) 90, https://doi.org/10.1007/s42452-019-1885-2.
[24] N. Banihashemi, J. Soltani-Nabipour, A. Khorshidi, H. Mohammadi, Quality control assessment of philips digital radiography and comparison with spellman and samsung systems in Tehran Oil Ministry Hospital, Eur. Phys. J. Plus 135 (2020), 269, https://doi.org/10.1140/epjp/s13360-020-00275-1. In press.
[25] A. Khorshidi, Exploration of adiabatic resonance crossing through neutron activator design for thermal and epithermal neutron formation in ^{99}Mo production and BNCT applications, Canc. Biother. Rad. 30 (8) (2015) 317–329, https://doi.org/10.1089/cbr.2014.1734.
[26] H. Tsujii, T. Kamada, A review of update: clinical results of carbon ion radiotherapy, Jpn. J. Clin. Oncol. 42 (8) (2012) 670–685, https://doi.org/10.1093/jjco/hys104.
[27] Y. Kumamoto, Y. Noda, Y. Sato, T. Kanai, T. Murakami, Measurements of neutron effective doses and attenuation lengths for shielding materials at the heavy-ion medical accelerator in Chiba, Health Phys. 88 (5) (2005) 469–479, https://doi.org/10.1097/01.hp.0000154026.39382.36.
[28] K. Gunzert-Marx, D. Schardt, R.S. Simon, Fast neutrons produced by nuclear fragmentation in treatment irradiations with 12C beam, Radiat. Protect. Dosim. 110 (1–4) (2004) 595–600, https://doi.org/10.1093/rpd/nch138.
[29] A. Khorshidi, Molybdenum-99 production via lead and bismuth moderators and milli-structure-98Mo samples by the indirect production technique using the Monte Carlo method, Phys. Usp. 62 (9) (2019) 931–940, https://doi.org/10.3367/UFNe.2018.09.038441.